ACS NANO

www.acsnano.org

ARTICLE

Stretchable and Smart Wettable Sensing Patch with Guided Liquid Flow for Multiplexed *in Situ* Perspiration Analysis

Yuping Sun, Jianhui Wang, Qianying Lu, Ting Fang, Shaolei Wang, Cheng Yang, Yong Lin, Qian Wang, Yan-qing Lu,* and Desheng Kong*

Cite This: *ACS Nano* 2024, 18, 2335−2345

Read Online

ACCESS | Metrics & More | Article Recommendations | Supporting Information

ABSTRACT: **Stretchable sweat sensors have become a personalized wearable platform for continuous, noninvasive health monitoring through conformal integration with the human body. Typically, these devices are coupled with soft microfluidic systems to control sweat flow during advanced analysis processes. However, the implementation of these soft microfluidic devices is limited by their high fabrication costs and the need for skin adhesives to block natural perspiration. To overcome these limitations, a stretchable and smart wettable patch has been proposed for multiplexed *in situ* perspiration analysis. The patch includes a porous membrane in the form of a patterned microfoam and a nanofiber layer laminate, which extracts sweat selectively from the skin and directs its continuous flow across the device. The integrated electrochemical sensor array measures multiple biomarkers simultaneously such as pH, K^+, and Na^+. The soft sensing patch comprises compliant materials and structures that allow deformability of up to 50% strain, which enables a stable and seamless interface with the curvilinear human body. During continuous physical exercise, the device has demonstrated a special operating mode by actively accumulating sweat from the skin for multiplex electrochemical analysis of biomarker profiles. The smart wettable membrane provides an affordable solution to address the sampling challenges of *in situ* perspiration analysis.**

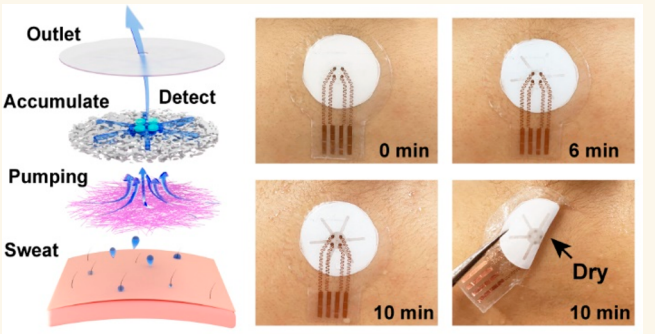

KEYWORDS: *sweat sensor, stretchable electronics, wettable, wearable sensor, electrochemical detection, multiplexed sensing*

INTRODUCTION

Wearable electronic gadgets that incorporate embedded sensors are revolutionizing the fields of fitness monitoring and clinical diagnosis.[1−6] However, traditional devices on rigid wafers struggle to establish stable interfaces with soft and dynamic skin surfaces for continuous measurements. To overcome this challenge, stretchable electronics have emerged as a disruptive technology to create sensors with compliant mechanical properties, enabling conformal integration with the curvilinear contours of the human body.[7,8] Currently, most research efforts focus on recording physical parameters such as skin temperature, body motions, heart rate, and blood pressure.[9−12] There is a rising frontier in analyzing biofluid biomarkers to probe the body's biomolecular state.[13−15] In particular, sweat is a convenient and noninvasive option for accessing abundant electrolytes and metabolites in the body. This benefit has led to the development of various skin-attached sweat sensors in the form of wristbands, temporary tattoos, and functional patches.[16] Colorimetric analysis is a low-cost technique that provides an immediate estimate of sweat compositions.[17,18] On the other hand, wearable electrochemical sensing devices often combine stretchable sensors with signal-processing circuitry, allowing real-time and multiplexed screening of target biomarkers.[19−22] Large sets of health data are easily acquired and can be coupled with big data tools to identify biomarkers for precision medicine.[23] This personalized analytical platform is therefore extremely attractive for advanced health monitoring, clinical diagnostics, and competitive sports.[16]

Received: October 21, 2023
Revised: December 28, 2023
Accepted: January 3, 2024
Published: January 8, 2024

https://doi.org/10.1021/acsnano.3c10324
ACS Nano 2024, 18, 2335−2345

Efficient sweat sampling is crucial for wearable sensors to achieve continuous and real-time measurements. Currently, sweat sensors are often paired with soft microfluidic systems for on-body biomarker detection.[18,24] Microfluidic channels and valves have proven to be highly effective in capturing and manipulating sweat on demand, essential for obtaining advanced measurements of sweat rate and biomarker profiles.[25−27] However, the widespread implementation of these microfluidic devices remains challenging due to their prohibitive microfabrication and labor-intensive manual assembly. In addition, soft microfluidic devices, predominantly constructed with low-modulus elastomers, are susceptible to severe deformations and irreversible collapses under external pressures. The careful optimization of the channel cross-section is often indispensable to enhance their robustness for practical wearable applications.[18] Moreover, microfluidic devices are known to lack an active sampling mechanism, leading to the accumulation of sweat at the skin−device interfaces. To mitigate this issue, adhesives are applied to affix the devices to the skin, with the opening at the microfluidic inlet to direct the sweat flow.[24,28] Nevertheless, the use of adhesives may block eccrine glands to induce compensatory sweating, which may alter the perspiration rate and chemical composition.[28−30] Long microfluidic channels and passive valves present in some microfluidic devices require an external driving force to operate, inducing pressure buildup on sweat glands.[25,28] To overcome these issues, porous absorbent materials such as paper, cotton, and silk have been used in wearable sweat sensors to accumulate sweat through capillary action.[31−34] Unfortunately, this primitive design faces the challenges of natural evaporation and uncontrolled intermixing of excreted sweat for quantitative analysis. Alternatively, bioinspired wettable materials have recently attracted significant attention due to their capability to manipulate fluids cost-effectively.[35,36] Two-dimensional superhydrophobic−superhydrophilic patterns effectively define the location and geometry of liquid droplets to control their interactions and reactions.[37,38] These patterned wettable films can concentrate sweat in wearable patches for colorimetric biomarker analysis.[17,39] Janus-wettable materials, on the other hand, are made up of stacked layers with opposite wettability that allow the spontaneous transportation of perspiration away from the body.[40−42] The Janus membrane can effectively facilitate sweat accumulation in wearable electrochemical sensors through unidirectional flow.[43] Despite these advancements, bioinspired wettable systems have yet to achieve the delicate control of complex sweat flow required for sustained biomarker detection during long-term physical exercise.

The study presents the design and fabrication of a stretchable sensing patch that can monitor multiple sweat biomarkers in real time. The device incorporates a bioinspired smart wettable membrane composed of patterned microfoam and a nanofiber layer laminate with engineered wettability gradients to manipulate sweat transport. The excreted sweat is continuously captured with vein-like channels, directed into the detection area, and discharged from the outlet. The continuous sweat flow reduces mixing risks and facilitates real-time measurements of its compositions. The patch has an integrated electrochemical sensor array that enables simultaneous measurement of various biomarkers, including pH, K^+, and Na^+. This patch utilizes compliant materials and structures, achieving skinlike deformability of up to 50% strain and conformal body integration. Additionally, the device has a distinctive operating mechanism that actively pumps sweat away from the skin without disrupting natural perspiration. We demonstrated the practical implementation of the sensing patch by performing real-time multiplexed measurements of sweat biomarkers during stationary cycling. The developments outlined in this study present an affordable material platform to address the sampling challenges of *in situ* perspiration analysis.

RESULTS AND DISCUSSION

As schematically illustrated in Figure 1a, the sensing patch comprises a stretchable electrochemical sensor array and a smart

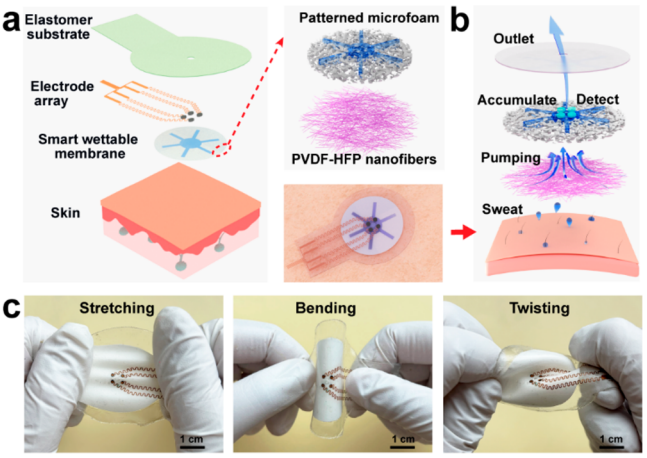

Figure 1. Design of the stretchable and smart wettable sensing patch. (a) Schematic illustration and optical image of a sweat-sensing patch attached to the skin. The patch is composed of a smart wettable membrane, a stretchable electrochemical sensor array, and an elastomer substrate. This membrane is a bilayer laminate of a patterned microfoam and PVDF-HFP nanofibers. (b) Schematic diagram illustrating the selective accumulation of sweat into the detection regions using the smart wettable membrane. (c) Mechanical manipulations of the sweat-sensing patch by stretching, bending, and twisting.

wettable membrane. The smart wettable membrane, consisting of a patterned microfoam and a nanofiber layer, is a crucial element of this device. Figure 1b displays a typical sensing patch attached to the skin. The remarkable capability of the smart wettable membrane is that it unidirectionally pumps secreted sweat into veinlike collection channels and a central detection area for electrochemical analysis. Any excess sweat is easily vented from the outlet port. This simplified design resembles conventional microfluidic systems to allow sweat to flow continuously through the sensing patch. In addition, the patch is constructed entirely based on compliant components, making it mechanically deformable and capable of withstanding various manipulations such as stretching, bending, and twisting (see Figure 1c).

The microfoam with patterned wettability has the ability to regulate the lateral flow of sweat. The fabrication of the microfoam involves blending salicylic acid microparticles (12 μm × 5 μm, see Figure S1) with the styrene−ethylene−butylene−styrene (SEBS) elastomer. The pores with a characteristic size of 9 μm are formed by leaching out these microparticles in ethanol (see Figure S2).[44] The resulting SEBS microfoam has a water contact angle of 123° (Figure 2a). Subsequently, fluorinated silica nanoparticles were assembled on the microfoam through ultrasonic immersion, leading to an increased water contact angle of 160°. Additional features of the

https://doi.org/10.1021/acsnano.3c10324
ACS Nano 2024, 18, 2335−2345

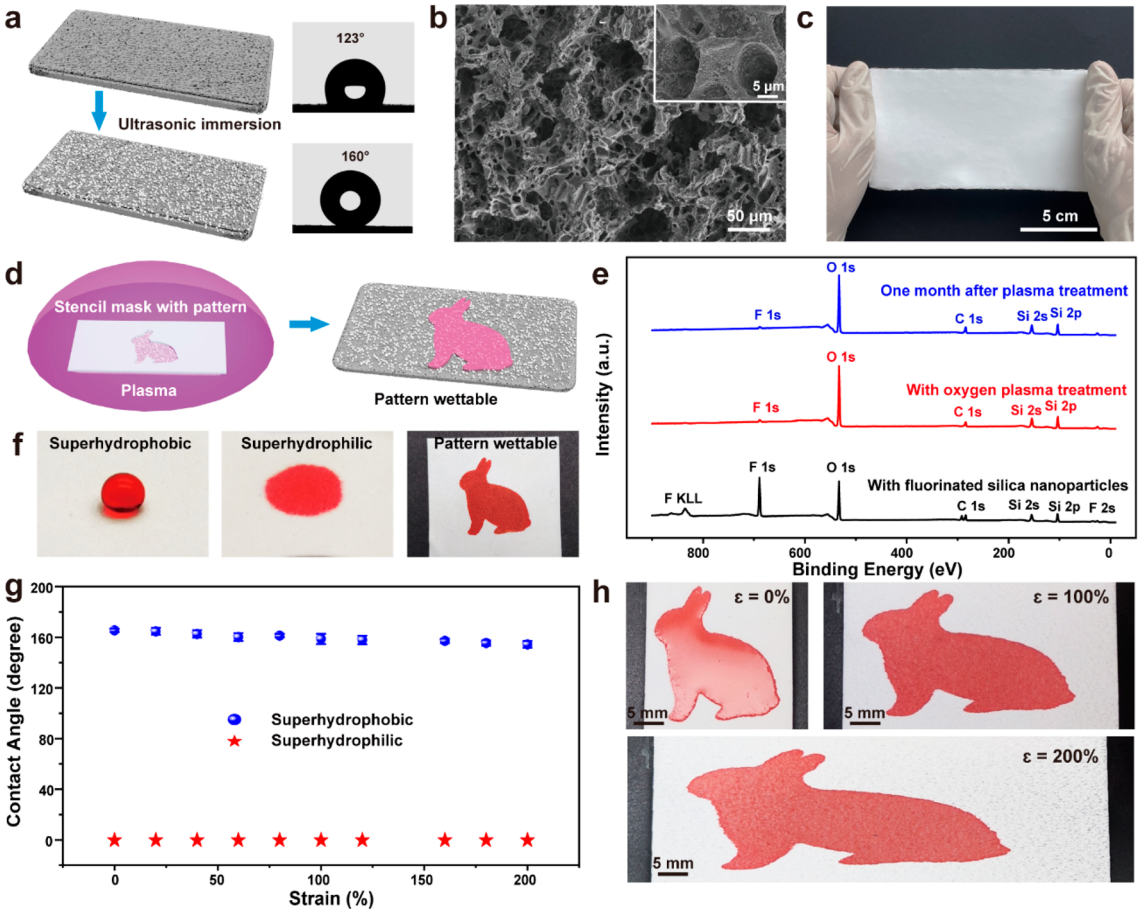

Figure 2. Patterned microfoams to control lateral sweat transport. (a) Preparation of superhydrophobic microfoams. (b) SEM image showing the porous microfoam decorated with fluorinated silica nanoparticles. (c) Optical image showing as-prepared superhydrophobic microfoams with compliant mechanical properties. (d) Schematic illustrating the fabrication of patterned wettability on the microfoam. (e) XPS spectra acquired from superhydrophobic microfoam with fluorinated silica nanoparticles, oxygen plasma-treated microfoam, and oxygen plasma-treated microfoam after one month of aging. (f) Wetting characteristics of water droplets on the superhydrophobic microfoam (left), superhydrophilic microfoam (middle), and patterned surface (right). (g) Water contact angle of the microfoam versus tensile strains. (h) Optical images showing absorbed water confined to the rabbit pattern under different tensile strains.

modified surface involve a small contact angle hysteresis of 1.4° and a low sliding angle of 2.1°, as shown in Figure S3, suggesting the lack of adhesion to water droplets. These superhydrophobic characteristics are attributed to heterarchical nano- and microstructures similar to those found on lotus leaves, which effectively trap air pockets and create a water-repellent effect.[45,46] In Figure 2b, the SEM image shows the relatively uniform decoration of fluorinated silica nanoparticles on the porous microfoam. The stretchy microfoams can be prepared over a large area, as demonstrated in Figure 2c. The patterned wettability in the microfoam is defined with a masked oxygen plasma technique according to Figure 2d. The oxygen plasma exposure significantly reduces the water contact angle of the microfoam to ~0° without affecting its porous structure (Figure S4). According to Figure 2e and Table S1, X-ray photoelectron spectroscopy (XPS) analysis shows a significant reduction of F 1s peaks due to the removal of fluorophobic silane chains through plasma treatment.[47] Additionally, the treatment introduces high-energy, oxygen-containing polar groups on the surface, as evidenced by increased oxygen atomic percentage from 33.1% to 54.4%.[48,49] However, this modified surface experiences hydrophobic recovery after one month, manifested as a notably increased water contact angle of 43° (Figure S5). This aging phenomenon is associated with the gradual restoration of the equilibrium surface, which is facilitated by the reorientation of the polar surface groups and the migration of small polymer segments.[50,51] XPS spectra confirm the significant decrease in oxygen atomic percentage after one month of storage (Table S1). To achieve long-term superhydrophilicity, the plasma-activated region is coated with a poly(vinyl alcolhol) (PVA) layer, as demonstrated in Figure S6. Interestingly, the PVA coating cannot be easily removed through repeated washing, as evidenced by Fourier transform infrared spectroscopy (FTIR) analyses in Figure S7 and XPS spectra in Figure S8. The PVA is known to attach to plasma-modified surfaces through hydrogen bonding irreversibly.[52,53] As a result, permanent modification of the microfoam surface through the PVA layer ensures durable superhydrophilicity. In sharp contrast, the stencil-masked regions of the microfoams are protected from the oxygen plasma, which helps to maintain their original superhydrophobic properties (see Figure 2f and Figure S9). The superhydrophobicity is also stable over extended periods (Figure S10).

In Figure 2f, water droplets are either completely repelled in the superhydrophobic region or irregularly absorbed in the superhydrophilic region. Notably, the superhydrophilic pattern on microfoam allows selective water absorption in a well-defined rabbit shape. The resolution of the wettability features can reach

https://doi.org/10.1021/acsnano.3c10324
ACS Nano 2024, 18, 2335−2345

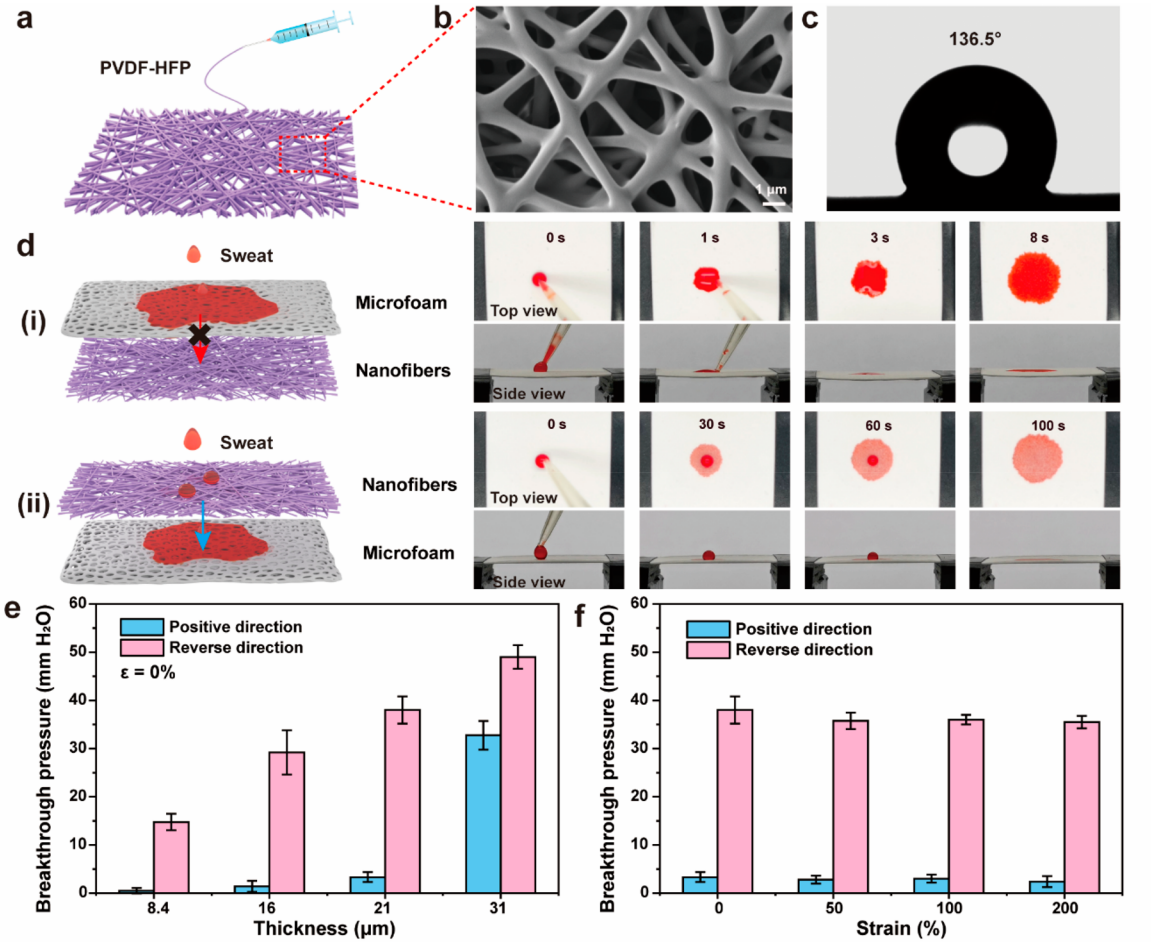

Figure 3. Janus membranes to manipulate vertical sweat transport. (a) Schematic diagram showing the preparation of the layer of PVDF-HFP nanofibers. (b) SEM image of the PVDF-HFP nanofibers. (c) Contact angle image of a water droplet on PVDF-HFP nanofibers. (d) (i) Optical images displaying a water droplet cast on the microfoam side of the Janus membrane that is absorbed without penetrating through the nanofiber layer; (ii) water droplets cast on the nanofiber side of the Janus membrane, which manage to penetrate through the nanofibers and get absorbed by the microfoam. (e) Anisotropic breakthrough pressure of the Janus membrane with the nanofiber layer at different thicknesses. (f) Anisotropic breakthrough pressure of the Janus membrane at different tensile strains. The nanofiber layer has a thickness of 21 μm.

up to 500 μm using this patterning approach, as illustrated in Figures S11 and S12. Despite the surface modifications, the patterned microfoam retains its compliant mechanical properties to accommodate large tensile deformation, as illustrated in Figure S13. The water contact angles of both superhydrophilic and superhydrophobic regions are stable for up to 200% strain (Figure 2g). As revealed in Figure S14, the overall micro/nanoscale structure of the microfoam is largely preserved despite some elongations of the micropores, thereby achieving strain-insensitive wettability.[54,55] For a proof-of-concept demonstration, the water droplet is drop cast on a patterned microfoam that is subjected to uniaxial tensile deformations. As shown in Figure 2h, the water droplet is well confined into the patterned rabbit feature during the stretching process, thanks to the significant wettability contrast to inhibit uncontrolled spreading.[17,39]

The Janus membrane allows directional sweat transport in the vertical direction. As schematically illustrated in Figure 3a, the membrane is prepared by electrospinning PVDF-HFP nanofibers over superhydrophilic microfoams. The SEM image in Figure 3b reveals that PVDF-HFP nanofibers are assembled in a nonwoven layer. According to the size distribution analysis in Figure S15, the electrospun nanofibers have an average diameter of ~700 nm. This nanofiber layer alone exhibits a characteristic water contact angle of 136.5°, as depicted in Figure 3c. These hydrophobic nanofibers can maintain a stable contact angle of up to 200% strain (Figure S16). Accordingly, the Janus membrane is a stretchable bilayer laminate based on components of distinctive wettability. When water droplets drop on the microfoam side of the Janus membrane, they spread immediately upon contact and get irregularly absorbed, as depicted in Figure 3d (i) and Movie S1. The nanofiber layer remained dry in this case. In contrast, the water droplet cast on the PVDF-HFP nanofibers initially remains spherical due to the pinning of the three-phase contact line (see Figure 3d (ii) and Movie S1). The light red wetting area gradually increases as the water droplet penetrates through nanofibers into the microfoam. The observed distinctive wetting behaviors suggest the unidirectional water transport of the Janus membrane along the nanofiber-to-microfoam direction, which is defined as the positive direction accordingly. As shown in Figure 3e, the reverse breakthrough pressure is always higher than the positive one for varying nanofiber thicknesses, consistent with liquid diode-like unidirectional transport. Increasing the nanofiber thickness extends the hydrophobic microchannels and in turn raises the breakthrough pressure values.[56] The high anisotropy

https://doi.org/10.1021/acsnano.3c10324
ACS Nano 2024, 18, 2335−2345

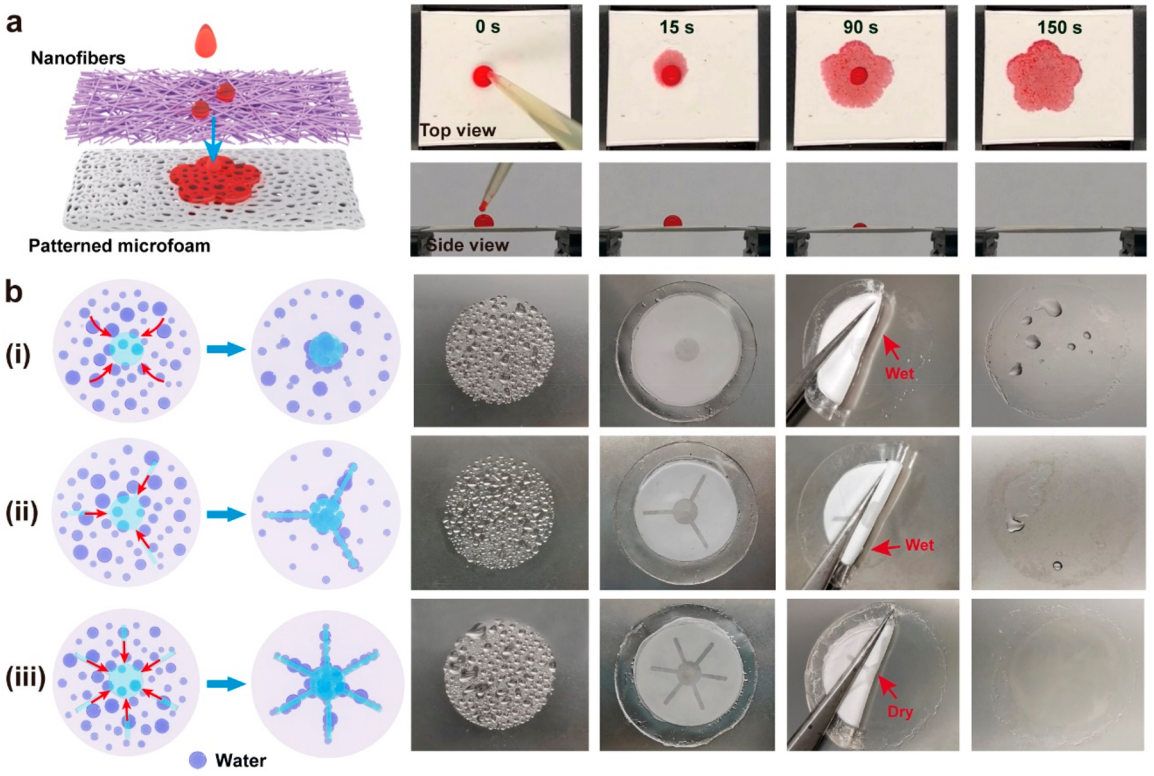

Figure 4. 3D sweat manipulation of the smart wettable membrane. (a) Schematic diagram (left) and optical images (right) showing the selective accumulation of water droplets in the flower-shaped pattern embedded in the smart membrane. (b) Demonstration of the sweat collection using different pattern designs with different channel numbers of smart wettable membranes.

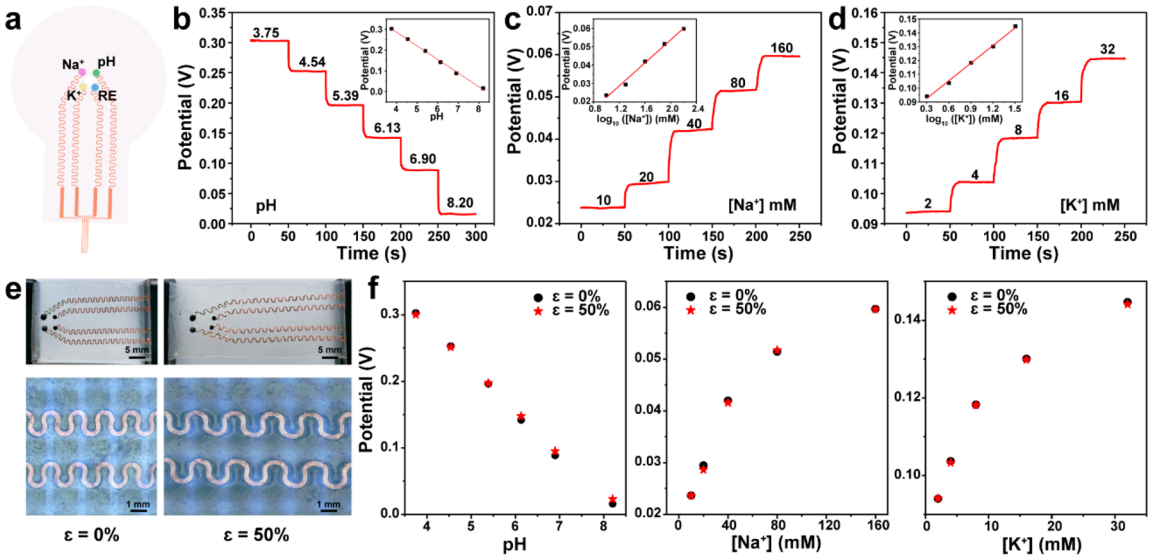

Figure 5. Characterizations of the stretchable sensor array. (a) Schematic diagram of the stretchable electrochemical sensor arrays. (b–d) Open-circuit potential responses of (b) pH, (c) Na^+, and (d) K^+ sensors in standard analytes. (e) Optical images of the stretchable sensor array at 0% (left) and 50% (right) strains. (f) Open-circuit potential responses of pH (left), Na^+ (middle), and K^+ (right) sensors at 0% and 50% strains.

at breakthrough pressures is well maintained until the nanofiber layer reaches 21 μm. This thickness is selected as the optimal design of the Janus membrane, exhibiting a high reverse breakthrough pressure of 38 mm H_2O and an order of magnitude pressure anisotropy. In addition to the relaxed state, the breakthrough pressure values slightly decrease during stretching due to the thickness reduction in the nanofiber layer (Figure S17). For example, the reverse breakthrough pressure is 35 mm H_2O at 200% strain. Fortunately, the pressure anisotropy is still well-preserved. The Janus membrane demonstrates reliable unidirectional transport under stretched conditions of up to 200% strain (Figure 3f).

The smart wettable membrane can manipulate sweat in three dimensions by combining patterned microfoam and electrospun nanofibers. The superhydrophilic features in the microfoam are effective collection areas for excreted sweat. In Figure 4a, water

https://doi.org/10.1021/acsnano.3c10324
ACS Nano 2024, 18, 2335−2345

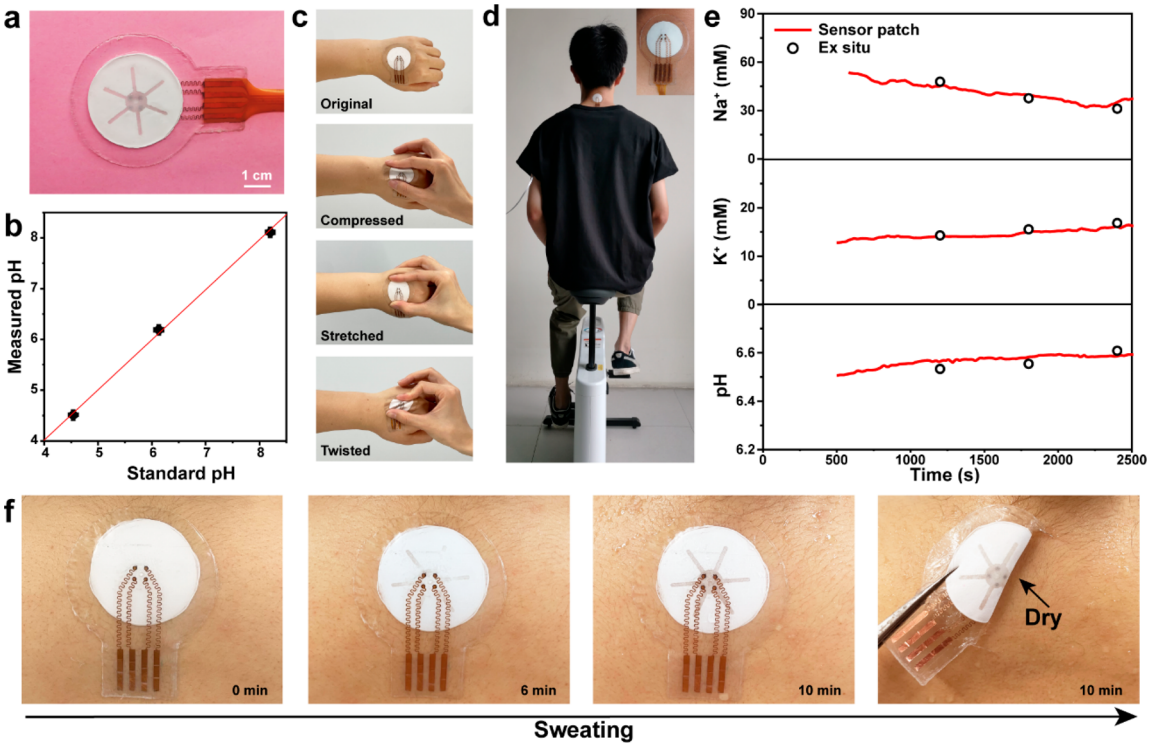

Figure 6. Skin-attached accumulation and analysis of sweat using the stretchable sensing patch during physical exercise. (a) Optical image of a representative stretchable sensing patch. (b) Comparison of the measured pH by the sensing patch with the pH value of the analyte. (c) Optical image showing a sensing patch mounted on the hand dorsum that maintains the conformal skin attachment under different manipulations. (d) Optical image of a subject wearing the sensing patch during stationary cycling. The inset shows that the patch is attached to the neck. (e) Real-time monitoring of sweat compositions during continuous cycling accomplished using the sensing patch. The sweat compositions are verified through postanalysis using standard techniques, as labeled by the hollow dots. (f) Optical images displaying the *in situ* sweat collection of the patch during continuous exercise.

droplets can be selectively concentrated into the flower feature in the microfoam by passing through nanofibers. An additional movie further reveals this on-demand collection process (Movie S2). According to Figure S18 and Movie S2, the nanofibers in the membrane act as a barrier that inhibits the backflow of collected sweat. This 3D transport capability is still well-preserved even after long-term storage, as demonstrated in Figure S19. Notably, the membrane's water transport capability remains stable when stretched to 200% strain (see Figure S20) and bent to different radii (Figure S21). Moreover, the membrane exhibits consistent breakthrough pressures, even after 200 bending cycles, as shown in Figure S22. The smart wettable membranes are further evaluated for their capability to collect sweat, as summarized in Figures 4b and S23. To simulate the skin after perspiration, a water spray of 120 mg was deposited on a stainless steel surface of ~9.6 cm^2. The results show that a membrane with only a central detection area fails to collect all water droplets on the surface, resulting in approximately 34 mg of residue (Figure 4b, i). The collection efficiency is calculated to be 71.7%. However, introducing veinlike collection channels alongside the central detection area helps in sweat extraction. The channels are symmetrically placed to maximize the collection capability. The membrane with three channels demonstrates improved water capture, leaving only ~12 mg of residue, as shown in Figure 4b (ii). The collection efficiency has a notable increase to 90%. Further increasing the number of channels to six allows the membrane to absorb almost all water on the contacting surface, leading to an exceptional collection efficiency exceeding 99% (Figure 4b, iii). These results suggest that a high channel count may facilitate the liquid to contact adjacent channels for thorough collection. Nevertheless, it is crucial to maintain a balance in the design of the collection channels to avoid an uncontrollable increase in their total area and the resulting trapped sweat. Achieving this balance is an optimal design strategy for effective sweat accumulation and analysis using the smart wettable membrane.

Stretchable electrochemical sensor arrays are created through a strain engineering approach. As schematically illustrated in Figure 5a, inextensible electrodes based on multiwalled carbon nanotube (MWCNT) nanocomposites are interconnected with serpentine copper wires to achieve stretchability at the system level. The pH-sensing electrode is created by electrochemically depositing polyaniline (PANI) over the MWCNT nanocomposite, which detects H^+ ions through protonation–deprotonation processes. The potentiometric sensing of Na^+ and K^+ levels is achieved by electrochemically depositing PEDOT:PSS over MWCNT composites as a signal transduction layer, followed by coating ion-selective membranes. In addition, a solid reference electrode comprising Ag/AgCl nanowires covered with a PVB-based electrolyte membrane provides a stable potential in solutions with varying ionic strengths. The fabrication of these electrodes is outlined in the Methods section and Supporting Figure S24. In Figure S25, SEM images reveal the microstructure of functional electrodes to confirm the successful modifications. The potentiometric sensors operate in a two-electrode configuration by coupling sensing electrodes to a common reference electrode. In Figure 5b–d, the sensors show open-circuit potentials (OCPs) in physiologically relevant

https://doi.org/10.1021/acsnano.3c10324
ACS Nano 2024, 18, 2335–2345

analytes in the range of 3.75 to 8.20 pH (Figure 5b), 1 to 160 mM Na^+ (Figure 5c), and 1 to 32 mM K^+ (Figure 5d). All sensors show linear relationships between the OCPs and logarithm of H^+, Na^+, and K^+ concentrations. The sensitivities are 65.7 mV/decade for the pH sensor, 31.3 mV/decade for the Na^+ sensor, and 42.5 mV/decade for the K^+ sensor. In addition, the stretchability of multiplexed sensor arrays is evaluated by uniaxial stretching. The optical images in Figure 5e reveal that the sensor array can easily endure up to 50% strain. The tensile deformations are almost entirely absorbed by the local unbending of serpentine interconnects, resulting in hardly any deformation on the stiff sensing electrodes. This stretchability level is sufficient for the maximal deformation experienced with the human skin.[57] As shown in Figure 5f, the OCPs of the sensors show negligible changes upon stretching to 50% strain. The sensitivities of this stretched sensor array are 63.2, 31.6, and 42.0 mV/decade for pH, Na^+, and K^+, respectively. The reliable responses during stretching are of paramount importance for the accurate quantification of analyte compositions.

The stretchable sensing patch is assembled by laminating the smart wettable membrane onto the multiplexed sensor array, as shown in Figure 6a. The sensing patch is evaluated with standard pH analytes as an example, which shows excellent consistency with the expected values (Figure 6b). With wearable applications in mind, the biocompatibility of the materials that come into contact with the skin has been verified through cell viability analyses, as summarized in Figure S26. The soft and stretchy patch is affixed to the human body by using silicone gel adhesive around the edge. Mechanical manipulation tests, as shown in Figure 6c, provide evidence that the sensing patch can maintain a stable attachment to the skin even under compressing, stretching, and twisting conditions. Furthermore, the smart wettable membrane is well-protected with the nonpermeable elastomer substrate and silicone gel adhesive, which effectively hinders unnecessary evaporation. *In situ*, continuous sweat analysis is carried out during stationary cycling on a constant-load ergometer (Figure 6d). The patch is conformally mounted on the neck of a human subject. In Figure S27, the sensor retains stable potential outputs under body movements, demonstrating its reliability for *in situ* sweat detection. Figure 6e reveals the real-time responses of the sensor array. To ensure reliable readings, the data collection starts at ~10 min in the cycling session when the detection area is fully soaked with excreted sweat. During the course of continuous exercise, there is a rise in sweat K^+ and a slight decrease in Na^+. Sweat pH remains relatively stable at around 6.5. To verify the accuracy of our patch measurements, the collected sweat is examined by commercial kits (Figure S28) or commercial electrodes. These *in situ* measured concentrations are consistent with those obtained through postanalysis using standard lab techniques, as shown in Figure 6e by hollow dots. The measured sweat compositions are within the expected ranges of healthy individuals.[16,58] In addition, sweat collection in the sensing patch is also carefully examined during physical exercise, as shown in Figure 6f. The excreted sweat gradually fills the collection channels and the detection area. The extra sweat is drained from the outlet ports, enabling continuous sweat transport across the device. The unidirectional vertical transport of sweat ensures a dry interface with the skin, which provides pleasant perceptions during long-term monitoring. As a desirable benefit, the selective accumulation of sweat into the detection area is driven by the wettability gradient without disrupting normal perspiration. The operation mode retains the standard physiology of the perspiration process for high-fidelity biomarker detections.

CONCLUSIONS

This study presents a stretchable electrochemical sensing patch that harnesses a smart wettable membrane to sample sweat for real-time and multiplexed biomarker detection. In a low-cost and scalable process, the bilayer porous membrane is created with an artificially engineered wettability distribution to selectively concentrate sweat into the central detection area and guide its flow continuously across the device. The electrochemical sensor array allows quantitative measurement of representative biomarkers, including pH, K^+, and Na^+. The sensing patch utilizes compliant materials and structures to maintain stable operations under mechanical deformations, making it conform to the curvilinear and dynamic contours of the human body. The device has enabled an attractive wearable form factor that actively extracts sweat under natural physiological conditions. The successful real-time analysis of multiple biomarker profiles illustrates the practical implementation of a sweat-sensing patch during continuous physical exercise. Importantly, we envision bioinspired smart wettable materials as a cost-effective platform to address sweat sampling challenges for next-generation skin-attached chemical sensors. Although the collection channels in these membranes enhance sweat accumulation, they end up absorbing a significant amount of excreted sweat. The improved resolution of wettability patterns on porous scaffolds is worth pursuing to reduce the extra waste involved in sweat sampling. While our device design is generally suitable for long-term sweat analysis, many electrochemical sensors are prone to drifts and failures during storage and continuous operation. Moving forward, the reliable detection of sweat compositions in skin-attached patches largely relies on breakthroughs in the shelf life and sensing stability of electrochemical sensors.

METHODS

Materials. All chemicals and raw materials were purchased from corresponding vendors, including SEBS (Tuftec H1052) from Asahi Kasei Elastomers, poly(vinylidene fluoride-*co*-hexafluoropropylene) (PVDF-HFP, DAI-EL G901) from Daikin Industries, 1*H*,1*H*,2*H*,2*H*-perfluorodecyltriethoxysilane (FAS), silica NPs (50 nm), 3,4-ethylenedioxythiophene (EDOT), poly(sodium 4-styrenesulfonate) (NaPSS), bis(2-ethylehexyl) sebacate (DOS), poly(vinyl butyral) (PVB, B-98), iron(III) chloride hexahydrate ($FeCl_3 \cdot H_2O$), NaCl, and KCl from Shanghai Macklin Biochemical Co., Ltd., EVA from DuPont, valinomycin, Na ionophore X, and sodium tetrakis[3,5-bis-(trifluoromethyl)phenyl] borate (Na-TFPB) from Shanghai Yuanye Biotechnology Co., Ltd., high-molecular-weight polyvinyl chloride (PVC) and aniline from Sigma-Aldrich Inc., diethyltetramethylimidazole (2E4MI) and E51epoxy resin from Shanghai Wandao Chemical Co., Ltd., polyether amine (JEFFAMINE D2000) from Huntsman, and MWCNTs (XFQ041) of 20−100 μm length and 10−20 nm diameter from Nanjing XFNANO Technology Co., Ltd. Other solvents and reagents were acquired from Nanjing Chemical Reagent Co., Ltd. The 3M Primer 94 was purchased from the 3M company. The fluorinated silica nanoparticles were prepared using a previously reported method.[59] Briefly, silica nanoparticles were ultrasonically dispersed in ethanol at a concentration of 1 w/w% for 15 min using a 900 W probe sonicator (ATPIO-900D, Nanjing Xianou Instrument Manufacturing Co., Ltd.). After adding FAS at 1% (w/w), the dispersion was further processed in a linear shaker for 8 h. The functionalized nanoparticles were thoroughly washed with ethanol to remove any excess FAS.

https://doi.org/10.1021/acsnano.3c10324
ACS Nano 2024, 18, 2335−2345

Fabrication of Patterned Microfoams. Salicylic acid microparticles of cuboid shapes were synthesized through antisolvent crystallization with characteristic dimensions of approximately 12 μm × 5 μm.[44] These microparticles were added to a SEBS solution (15 w/w % in toluene) as the sacrificial template in a mass ratio of 1:3 and then homogenized in an FS400-ST laboratory blender from Shanghai Lichen-BX Instrument Technology Co., Ltd. The resulting viscous mixture was blade-cast into composite films on nonsticky glass wafers. The SEBS microfoams were generated after the embedded salicylic acid microparticles were dissolved in ethanol for 4 h. The pores have a dominant distribution of ∼9 μm and a small fraction of 35 μm. To improve the water repellent characteristics, the SEBS microfoam was immersed in a fluorinated silica nanoparticle dispersion (1 w/w% in ethyl alcohol) and underwent ultrasonic treatment for 5 min to facilitate nanoparticle assembly. The subsequent annealing at 80 °C improved the interface adhesion between the silica nanoparticles and SEBS microfoams. This process was repeated four times to ensure an adequate nanoparticle coverage. To produce patterned wettability, the microfoam covered with a machined acrylic shadow mask was placed inside a Mingheng PDC-MG plasma cleaner for an oxygen plasma treatment for 5 min. The acrylic shadow mask was pressed against the substrate surface with binder clips to obtain accurate patterns. A layer of PVA was coated on the plasma-activated region to achieve long-term superhydrophilicity by soaking with a 2 w/w% PVA aqueous solution.

Fabrication of Janus Membranes and Smart Wettable Membranes. PVDF-HFP was dissolved in methyl isobutyl ketone at 10 w/w% and filled in a 20 mL syringe with a 23 G stainless steel dispensing needle. The polymer solution was delivered into the needle at a rate of 1.5 mL/h by using a TYD01-01 syringe pump from Lead Fluid Technology Co., Ltd. The needle was placed at a fixed distance of 20 cm from a grounded aluminum foil collector and subjected to a high voltage of 15 kV. Accordingly, the polymer solution was electrostatically drawn into nanofibers with a diameter of ∼700 nm and deposited onto aluminum foil. Janus membranes were produced by placing superhydrophilic microfoams on the aluminum foil collector, whereas smart wettable membranes were generated by placing patterned microfoams on the collector. The nanofiber layer thickness was adjusted by varying the electrospinning duration.

Fabrication of Stretchable Electrochemical Sensor Arrays. The SEBS substrate was prepared by drop casting its solution (20 w/w % in toluene) on a nonsticky glass wafer and then allowing it to dry under ambient conditions. An EVA layer was spin-coated onto a fluoroplastic film and then thermally laminated on the SEBS substrate as a bonding layer. The copper-clad polyimide film was attached to a water-soluble tape and patterned through selective laser ablation using a 1064 nm fiber laser marking system from Shanghai Diaotu Industrial Co., Ltd. After surface modification with 3M Primer 94, the patterned polyimide film was thermally laminated onto the elastomer substrate. The water-soluble tape was subsequently removed in deionized water. The Cu interconnects were selectively modified with 3M Primer 94 and bonded to an EVA layer for encapsulation. A conductive nanocomposite slurry was prepared by mixing E51 epoxy resin, poly(ether amine), MWCNTs, and 2E4MI at a ratio of 100:10:7:5. The slurry was stencil printed into 1.2 mm dots on Cu contact pads and thermally cured at 100 °C inside an oven for 2 h. As regards the common reference electrode, the fabrication protocol begins with synthesizing Ag/AgCl nanowires. Silver nanowires (Ag NWs) were grown through a polyol reduction method.[58,60] These Ag NWs were chlorinated using a previously reported method.[61] Briefly, a Ag NW dispersion in 2-propanol was dissolved with 6 mg/mL PVP. A 50 μL amount of a 20 mM $FeCl_3$ solution was added dropwise to the dispersion under constant stirring every 5 s for 3 min. The resulting Ag/AgCl nanowires were washed and redispersed in isopropyl alcohol. The Ag/AgCl dispersion was drop cast on the nanocomposite electrode. A solid electrolyte membrane was then generated by drop casting the precursor solution comprising 79.1 mg of PVB, 50 mg of NaCl, and 0.2 mg of MWCNT dissolved in 1 mL of methanol. The pH-sensing electrode was created by electroplating PANI on the nanocomposite electrode. The cyclic voltammetric deposition was carried out in an aqueous solution containing 0.1 M aniline and 1 M HCl, using an electrochemical workstation (ChenHua China). The protocol to prepare K^+- and Na^+-sensing electrodes involves preparing two types of ion-selective membrane cocktails. The first one for K^+ selection was made by mixing 2 w/w% valinomycin, 0.5 w/w% NaTPB, 32.7 w/w% PVC, and 64.7 w/w% DOS. This cocktail of 100 mg was then dissolved in 350 μL of cyclohexanone. The second one for Na^+ selection was made by mixing 1 w/w% Na ionophore X, 0.55 w/w% Na-TFPB, 33 w/w% PVC, and 65.45 w/w% DOS. This membrane cocktail of 100 mg was dissolved in 660 μL of tetrahydrofuran. These solutions were then sealed and stored at 4 °C until further use. Next, PEDOT:PSS was electrodeposited onto the nanocomposite electrodes as an ion-electron transducer layer. The cyclic voltammetric deposition was carried out in an aqueous solution containing 0.01 M EDOT and 0.1 M NaPSS. Ion-selective electrodes were created by drop-casting 2 μL of ion-selective cocktail solution onto PEDOT/PSS-modified electrodes, followed by drying at room temperature for more than 12 h. The fabricated ion selective electrodes need preconditioning in a solution of 0.01 M KCl and 0.1 M NaCl for 1 h before the measurements to enhance their stability.

Fabrication of the Sweat-Sensing Patch and On-Body Sweat Analysis. An electrochemical sensor array on a SEBS elastomer substrate had a 1-mm-diameter hole drilled at the center as the sweat outlet using a CO_2 laser marking system from Liaocheng Jingwei Laser Technology Co., Ltd. The entire device except for the active electrodes was brush-painted with a silicone gel adhesive (Silbione RT gel 4645A/B, Elkem Silicones). To facilitate the alignment, a smart wettable membrane had superhydrophilic regions revealed by drop casting with deionized water. The membrane was then pressed against the sensing device to ensure tight bonding. The membrane was intentionally made smaller than the overall device, leaving silicone gel adhesive around the edge to allow for skin attachment. Written informed consent was obtained from all human subjects who participated in on-body testing. The skin was cleansed using alcohol swabs to remove any contaminants. The sensing patch was attached to the back of the neck and then wired with the electrochemical workstation. Constant workload cycling was conducted on a Merach exercise bike for ∼40 min. Once sufficient sweat had accumulated in the detection region, the sensor produced stable readings to signify the beginning of continuous data recording. The *in situ* measurements were verified using the standard sweat testing method. Specifically, a piece of medical gauze was placed adjacent to the patch to absorb sweat and covered completely with plastic wrap to prevent evaporation. The gauze was replaced every 10 min. The sweat was extracted from each soaked gauze via centrifugation at 10 000 rpm for 10 min in a centrifugal filter tube. The concentrations of Na^+ and K^+ were determined through colorimetric analysis using a Thermo Scientific Varioskan Flash reader and standard kits from the Nanjing Jiancheng Bioengineering Institute. Additionally, the pH was measured with a LabSen241-3S micro pH electrode from Shanghai Huxi Instrument Equipment Co., Ltd.

Biocompatibility Assessment of the Sweat-Sensing Patch. *In vitro* biocompatibility of material components that come into contact with the skin was assessed using the embryonic mouse fibroblast cell line NIH-3T3 from the American Type Culture Collection. NIH-3T3 cells were seeded in 96-well plates (∼10 000 per well) using DMEM medium supplemented with 10% fetal bovine serum and 1% penicillin/streptomycin. After overnight incubation at 37 °C, the culture medium was replaced with 200 μL of fresh medium containing the testing sample, such as silicone gel adhesive, PVDF-HFP elastomer, and PVDF-HFP nanofibers. The plates were then incubated for 48 h. Subsequently, the culture medium was replaced with 100 μL of fresh medium and supplemented with 10 μL of CCK-8 solution. After an additional 2 h of incubation, cell viability was determined with the absorbance at 450 nm measured using a Tecan Infinite 200 Pro microplate reader.

Characterizations. Optical images were captured by using a Fujifilm X-T10 camera. SEM images were acquired with a Zeiss Gemini 500 field emission scanning electron microscope. XPS spectra were acquired with a Thermo Scientific K-Alpha. Stress−strain curves were obtained by using a Shimadzu AGS-X universal testing machine with a 50 N load cell. FTIR spectra were acquired with a Thermo Nicolet 6700

https://doi.org/10.1021/acsnano.3c10324
ACS Nano 2024, 18, 2335−2345

spectrometer. Contact angle images were obtained with a DataPhysics OCA30 instrument. Potentiometric measurements of electrochemical sensors were carried out using the electrochemical workstation in two-electrode configurations.

ASSOCIATED CONTENT

Supporting Information

The Supporting Information is available free of charge at https://pubs.acs.org/doi/10.1021/acsnano.3c10324.

Characterizations of salicylic acid microparticles, additional water contact angle measurements, SEM image of superhydrophilic microfoams, FTIR and XPS acquired from the microfoams, characterizations on the patterning resolution, uniaxial stress−strain curves of different microfoams, SEM images of stretched microfoams, the diameter distribution of nanofibers, unidirectional water transport in stretched Janus membranes, 3D water transport capability of the smart wettable membrane after long-term storage and under mechanical deformations, the residual water left on the stainless steel surface after collecting with the smart wettable membrane, the process flows to create ion-selective electrodes, SEM images showing functional layers of ion-selective electrodes, *in situ* sweat detection during body movements, surface compositions based on XPS spectra, *in vitro* biocompatibility test, calibration curves for colorimetric analysis, and the pore size distribution of the microfoam (PDF)

Movie S1: Top and side-view movies of a water droplet cast on the microfoam and nanofiber sides of the Janus membrane (MP4)

Movie S2: Top and side-view movies of a water droplet cast on the patterned microfoam and nanofiber sides of the smart wettable membrane (MP4)

AUTHOR INFORMATION

Corresponding Authors

Desheng Kong − *College of Engineering and Applied Sciences, National Laboratory of Solid State Microstructure, and Collaborative Innovation Center of Advanced Microstructures, Nanjing University, Nanjing 210093, China; State Key Laboratory of Analytical Chemistry for Life Science, and Jiangsu Key Laboratory of Artificial Functional Materials, Nanjing University, Nanjing 210023, China;* orcid.org/0000-0002-7339-7593; Email: dskong@nju.edu.cn

Yan-qing Lu − *College of Engineering and Applied Sciences, National Laboratory of Solid State Microstructure, and Collaborative Innovation Center of Advanced Microstructures, Nanjing University, Nanjing 210093, China; Key Laboratory of Intelligent Optical Sensing and Manipulation, Nanjing University, Nanjing 210093, China;* orcid.org/0000-0001-6151-8557; Email: yqlu@nju.edu.cn

Authors

Yuping Sun − *College of Engineering and Applied Sciences, National Laboratory of Solid State Microstructure, and Collaborative Innovation Center of Advanced Microstructures, Nanjing University, Nanjing 210093, China; State Key Laboratory of Analytical Chemistry for Life Science, and Jiangsu Key Laboratory of Artificial Functional Materials, Nanjing University, Nanjing 210023, China*

Jianhui Wang − *College of Engineering and Applied Sciences, National Laboratory of Solid State Microstructure, and Collaborative Innovation Center of Advanced Microstructures, Nanjing University, Nanjing 210093, China; State Key Laboratory of Analytical Chemistry for Life Science, and Jiangsu Key Laboratory of Artificial Functional Materials, Nanjing University, Nanjing 210023, China*

Qianying Lu − *College of Engineering and Applied Sciences, National Laboratory of Solid State Microstructure, and Collaborative Innovation Center of Advanced Microstructures, Nanjing University, Nanjing 210093, China; State Key Laboratory of Analytical Chemistry for Life Science, and Jiangsu Key Laboratory of Artificial Functional Materials, Nanjing University, Nanjing 210023, China*

Ting Fang − *College of Engineering and Applied Sciences, National Laboratory of Solid State Microstructure, and Collaborative Innovation Center of Advanced Microstructures, Nanjing University, Nanjing 210093, China; State Key Laboratory of Analytical Chemistry for Life Science, and Jiangsu Key Laboratory of Artificial Functional Materials, Nanjing University, Nanjing 210023, China*

Shaolei Wang − *College of Engineering and Applied Sciences, National Laboratory of Solid State Microstructure, and Collaborative Innovation Center of Advanced Microstructures, Nanjing University, Nanjing 210093, China; State Key Laboratory of Analytical Chemistry for Life Science, and Jiangsu Key Laboratory of Artificial Functional Materials, Nanjing University, Nanjing 210023, China*

Cheng Yang − *College of Engineering and Applied Sciences, National Laboratory of Solid State Microstructure, and Collaborative Innovation Center of Advanced Microstructures, Nanjing University, Nanjing 210093, China; State Key Laboratory of Analytical Chemistry for Life Science, and Jiangsu Key Laboratory of Artificial Functional Materials, Nanjing University, Nanjing 210023, China*

Yong Lin − *College of Engineering and Applied Sciences, National Laboratory of Solid State Microstructure, and Collaborative Innovation Center of Advanced Microstructures, Nanjing University, Nanjing 210093, China; State Key Laboratory of Analytical Chemistry for Life Science, and Jiangsu Key Laboratory of Artificial Functional Materials, Nanjing University, Nanjing 210023, China*

Qian Wang − *College of Engineering and Applied Sciences, National Laboratory of Solid State Microstructure, and Collaborative Innovation Center of Advanced Microstructures, Nanjing University, Nanjing 210093, China; State Key Laboratory of Analytical Chemistry for Life Science, and Jiangsu Key Laboratory of Artificial Functional Materials, Nanjing University, Nanjing 210023, China;* orcid.org/0000-0001-8756-1422

Complete contact information is available at: https://pubs.acs.org/10.1021/acsnano.3c10324

Author Contributions

The manuscript was written through contributions of all authors. All authors have given approval to the final version of the manuscript. Y.S. and J.W. contributed equally to this work.

Notes

The authors declare no competing financial interest.

ACKNOWLEDGMENTS

We acknowledge the support from the National Key Research and Development Program of China (Grant No. 2022YFA1405000), the Natural Science Foundation of Jiangsu

Province, Major Project (Grant No. BK20212004), the National Natural Science Foundation of China (Grant No. 62374083), and the State Key Laboratory of Analytical Chemistry for Life Science (Grant No. 5431ZZXM2205).

REFERENCES

(1) Yang, J. C.; Mun, J.; Kwon, S. Y.; Park, S.; Bao, Z.; Park, S. Electronic Skin: Recent Progress and Future Prospects for Skin-Attachable Devices for Health Monitoring, Robotics, and Prosthetics. *Adv. Mater.* **2019**, *31*, No. e1904765.
(2) Wang, X.; Zheng, L.; Ting, Z. Flexible Sensing Electronics for Wearable/Attachable Health Monitoring. *Small* **2017**, *13*, 1602790.
(3) Kim, J.; Campbell, A. S.; de Avila, B. E.; Wang, J. Wearable Biosensors for Healthcare Monitoring. *Nat. Biotechnol.* **2019**, *37*, 389−406.
(4) Yang, H.; Qian, Z.; Wang, J.; Feng, J.; Tang, C.; Wang, L.; Guo, Y.; Liu, Z.; Yang, Y.; Zhang, K.; Chen, P.; Sun, X.; Peng, H. Carbon Nanotube Array-Based Flexible Multifunctional Electrodes to Record Electrophysiology and Ions on the Cerebral Cortex in Real Time. *Adv. Funct. Mater.* **2022**, *32*, 2204794.
(5) Zhang, J.; Li, Y.; Chai, F.; Li, Q.; Wang, D.; Liu, L.; Tang, B. Z.; Jiang, X. Ultrasensitive Point-of-Care Biochemical Sensor Based on Metal-AIEgen Frameworks. *Sci. Adv.* **2022**, *8*, No. eabo1874.
(6) Libanori, A.; Chen, G.; Zhao, X.; Zhou, Y.; Chen, J. Smart Textiles for Personalized Healthcare. *Nat. Electron.* **2022**, *5*, 142−156.
(7) John, A.; Rogers, T. S.; Yonggang, H. Materials and Mechanics for Stretchable Electronics. *Science* **2010**, *327*, 1603−607.
(8) Zhong, L.; Tang, L.; Yang, S.; Zhao, Z.; Zheng, Z.; Jiang, X. Stretchable Liquid Metal-Based Metal-Polymer Conductors for Fully Screen-Printed Biofuel Cells. *Anal. Chem.* **2022**, *94*, 16738−16745.
(9) Luo, Y.; Abidian, M. R.; Ahn, J. H.; Akinwande, D.; Andrews, A. M.; Antonietti, M.; Bao, Z.; Berggren, M.; Berkey, C. A.; Bettinger, C. J.; Chen, J.; Chen, P.; Cheng, W.; Cheng, X.; Choi, S. J.; Chortos, A.; Dagdeviren, C.; Dauskardt, R. H.; Di, C. A.; Dickey, M. D.; et al. Technology Roadmap for Flexible Sensors. *ACS Nano* **2023**, *17*, 5211−5295.
(10) Kim, D. H.; Lu, N.; Ma, R.; Kim, Y. S.; Kim, R. H.; Wang, S.; Wu, J.; Won, S. M.; Tao, H.; Islam, A.; Yu, K. J.; Kim, T.; Chowdhury, R.; Ying, M.; Xu, L.; Li, M.; Chung, H. J.; Keum, H.; McCormick, M.; Liu, P.; et al. Epidermal Electronics. *Science* **2011**, *333*, 838−843.
(11) Boutry, C. M.; Beker, L.; Kaizawa, Y.; Vassos, C.; Tran, H.; Hinckley, A. C.; Pfattner, R.; Niu, S.; Li, J.; Claverie, J.; Wang, Z.; Chang, J.; Fox, P. M.; Bao, Z. Biodegradable and Flexible Arterial-Pulse Sensor for the Wireless Monitoring of Blood flow. *Nat. Biomed. Eng.* **2019**, *3*, 47−57.
(12) Meng, K.; Xiao, X.; Wei, W.; Chen, G.; Nashalian, A.; Shen, S.; Xiao, X.; Chen, J. Wearable Pressure Sensors for Pulse Wave Monitoring. *Adv. Mater.* **2022**, *34*, No. e2109357.
(13) Yang, Y.; Gao, W. Wearable and Flexible Electronics for Continuous Molecular Monitoring. *Chem. Soc. Rev.* **2019**, *48*, 1465−1491.
(14) Li, X.; Huang, X.; Mo, J.; Wang, H.; Huang, Q.; Yang, C.; Zhang, T.; Chen, H. J.; Hang, T.; Liu, F.; Jiang, L.; Wu, Q.; Li, H.; Hu, N.; Xie, X. A Fully Integrated Closed-Loop System Based on Mesoporous Microneedles-Iontophoresis for Diabetes Treatment. *Adv. Sci.* **2021**, *8*, No. e2100827.
(15) Mou, L.; Xia, Y.; Jiang, X. Epidermal Sensor for Potentiometric Analysis of Metabolite and Electrolyte. *Anal. Chem.* **2021**, *93*, 11525−11531.
(16) Bariya, M.; Nyein, H. Y. Y.; Javey, A. Wearable Sweat Sensors. *Nat. Electron.* **2018**, *1*, 160−171.
(17) Zhang, K.; Zhang, J.; Wang, F.; Kong, D. Stretchable and Superwettable Colorimetric Sensing Patch for Epidermal Collection and Analysis of Sweat. *ACS Sens* **2021**, *6*, 2261−2269.
(18) Koh, A.; Kang, D.; Xue, Y.; Lee, S.; Pielak, R. M.; Kim, J.; Hwang, T.; Min, S.; Banks, A.; Bastien, P.; Manco, M. C.; Wang, L.; Ammann, K. R.; Jang, K. I.; Won, P.; Han, S.; Ghaffari, R.; Paik, U.; Slepian, M. J.; Balooch, G.; et al. A Soft, Wearable Microfluidic Device for the Capture, Storage, and Colorimetric Sensing of Sweat. *Sci. Transl. Med.* **2016**, *8*, 366ra165.
(19) Yang, Y.; Song, Y.; Bo, X.; Min, J.; Pak, O. S.; Zhu, L.; Wang, M.; Tu, J.; Kogan, A.; Zhang, H.; Hsiai, T. K.; Li, Z.; Gao, W. A Laser-Engraved Wearable Sensor for Sensitive Detection of Uric Acid and Tyrosine in Sweat. *Nat. Biotechnol.* **2020**, *38*, 217−224.
(20) Imani, S.; Bandodkar, A. J.; Mohan, A. M. V.; Kumar, R.; Yu, S.; Wang, J.; Mercier, P. P. A Wearable Chemical-Electrophysiological Hybrid Biosensing System for Real-Time Health and Fitness Monitoring. *Nat. Commun.* **2016**, *7*, 11650.
(21) Gao, W.; Emaminejad, S.; Nyein, H. Y. Y.; Challa, S.; Chen, K.; Peck, A.; Fahad, H. M.; Ota, H.; Shiraki, H.; Kiriya, D.; Lien, D. H.; Brooks, G. A.; Davis, R. W.; Javey, A. Fully Integrated Wearable Sensor Arrays for Multiplexed in Situ Perspiration Analysis. *Nature* **2016**, *529*, 509−514.
(22) Bandodkar, A. J.; Gutruf, P.; Choi, J.; Lee, K. H.; Sekine, Y.; Reeder, J. T.; Jeang, W. J.; Aranyosi, A. J.; Lee, S. P.; Model, J. B.; Ghaffari, R.; Su, C. J.; Leshock, J. P.; Ray, T.; Verrillo, A.; Thomas, K.; Krishnamurthi, V.; Han, S.; Kim, J.; Krishnan, S.; et al. Battery-free, Skin-interfaced Microfluidic/Electronic Systems for Simultaneous Electrochemical, Colorimetric, and Volumetric Analysis of Sweat. *Sci. Adv.* **2019**, *5*, No. eaav3294.
(23) Sempionatto, J. R.; Lasalde-Ramirez, J. A.; Mahato, K.; Wang, J.; Gao, W. Wearable Chemical Sensors for Biomarker Discovery in the Omics Era. *Nat. Rev. Chem.* **2022**, *6*, 899−915.
(24) Martin, A.; Kim, J.; Kurniawan, J. F.; Sempionatto, J. R.; Moreto, J. R.; Tang, G.; Campbell, A. S.; Shin, A.; Lee, M. Y.; Liu, X.; Wang, J. Epidermal Microfluidic Electrochemical Detection System: Enhanced Sweat Sampling and Metabolite Detection. *ACS Sens.* **2017**, *2*, 1860−1868.
(25) Choi, J.; Kang, D.; Han, S.; Kim, S. B.; Rogers, J. A. Thin, Soft, Skin-Mounted Microfluidic Networks with Capillary Bursting Valves for Chrono-Sampling of Sweat. *Adv. Healthc. Mater.* **2017**, *6*, 1601355.
(26) Lin, H.; Tan, J.; Zhu, J.; Lin, S.; Zhao, Y.; Yu, W.; Hojaiji, H.; Wang, B.; Yang, S.; Cheng, X.; Wang, Z.; Tang, E.; Yeung, C.; Emaminejad, S. A Programmable Epidermal Microfluidic Valving System for Wearable Biofluid Management and Contextual Biomarker Analysis. *Nat. Commun.* **2020**, *11*, 4405.
(27) Xiao, J.; Liu, Y.; Su, L.; Zhao, D.; Zhao, L.; Zhang, X. Microfluidic Chip-Based Wearable Colorimetric Sensor for Simple and Facile Detection of Sweat Glucose. *Anal. Chem.* **2019**, *91*, 14803−14807.
(28) Reeder, J. T.; Choi, J.; Xue, Y.; Gutruf, P.; Hanson, J.; Liu, M.; Ray, T.; Bandodkar, A. J.; Avila, R.; Xia, W.; Krishnan, S.; Xu, S.; Barnes, K.; Pahnke, M.; Ghaffari, R.; Huang, Y.; Rogers, J. A. Waterproof, Electronics-Enabled, Epidermal Microfluidic Devices for Sweat Collection, Biomarker Analysis, and Thermography in Aquatic Settings. *Sci. Adv.* **2019**, *5*, No. eaau6356.
(29) Licht, P. B.; Pilegaard, H. K. Severity of Compensatory Sweating after Thoracoscopic Sympathectomy. *Ann. Thorac. Surg.* **2004**, *78*, 427−31.
(30) Zhong, B.; Jiang, K.; Wang, L.; Shen, G. Wearable Sweat Loss Measuring Devices: From the Role of Sweat Loss to Advanced Mechanisms and Designs. *Adv. Sci.* **2022**, *9*, No. e2103257.
(31) He, X.; Fan, C.; Xu, T.; Zhang, X. Biospired Janus Silk E-Textiles with Wet-Thermal Comfort for Highly Efficient Biofluid Monitoring. *Nano Lett.* **2021**, *21*, 8880−8887.
(32) Mogera, U.; Guo, H.; Namkoong, M.; Rahman, M. S.; Nguyen, T.; Tian, Li. Wearable Plasmonic Paper-Based Microfluidics for Continuous Sweat Analysis. *Sci. Adv.* **2022**, *8*, No. eabn1736.
(33) Wang, L.; Lu, J.; Li, Q.; Li, L.; He, E.; Jiao, Y.; Ye, T.; Zhang, Y. A Core-Sheath Sensing Yarn-Based Electrochemical Fabric System for Powerful Sweat Capture and Stable Sensing. *Adv. Funct. Mater.* **2022**, *32*, 2200922.
(34) Tat, T.; Chen, G.; Zhao, X.; Zhou, Y.; Xu, J.; Chen, J. Smart Textiles for Healthcare and Sustainability. *ACS Nano* **2022**, *16*, 13301−13313.
(35) Xu, T.; Xu, L. P.; Zhang, X.; Wang, S. Bioinspired Superwettable Micropatterns for Biosensing. *Chem. Soc. Rev.* **2019**, *48*, 3153−3165.

https://doi.org/10.1021/acsnano.3c10324
ACS Nano 2024, 18, 2335−2345

(36) Liu, M.; Wang, S.; Jiang, L. Nature-Inspired Superwettability Systems. *Nat. Rev. Mater.* **2017**, *2*, 17036.
(37) Feng, W.; Ueda, E.; Levkin, P. A. Droplet Microarrays: From Surface Patterning to High-Throughput Applications. *Adv. Mater.* **2018**, *30*, No. e1706111.
(38) He, X.; Xu, T.; Gao, W.; Xu, L. P.; Pan, T.; Zhang, X. Flexible Superwettable Tapes for On-Site Detection of Heavy Metals. *Anal. Chem.* **2018**, *90*, 14105−14110.
(39) He, X.; Xu, T.; Gu, Z.; Gao, W.; Xu, L. P.; Pan, T.; Zhang, X. Flexible and Superwettable Bands as a Platform toward Sweat Sampling and Sensing. *Anal. Chem.* **2019**, *91*, 4296−4300.
(40) Xu, Y.; Guo, W.; Zhou, S.; Yi, H.; Yang, G.; Mei, S.; Zhu, K.; Wu, H.; Li, Z. Bioinspired Perspiration-Wicking Electronic Skins for Comfortable and Reliable Multimodal Health Monitoring. *Adv. Funct. Mater.* **2022**, *32*, 2200961.
(41) Yang, X.; Wang, S.; Liu, M.; Li, L.; Zhao, Y.; Wang, Y.; Bai, Y.; Lu, Q.; Xiong, Z.; Feng, S.; Zhang, T. All-Nanofiber-Based Janus Epidermal Electrode with Directional Sweat Permeability for Artifact-Free Biopotential Monitoring. *Small* **2022**, *18*, No. e2106477.
(42) Dai, B.; Li, K.; Shi, L.; Wan, X.; Liu, X.; Zhang, F.; Jiang, L.; Wang, S. Bioinspired Janus Textile with Conical Micropores for Human Body Moisture and Thermal Management. *Adv. Mater.* **2019**, *31*, No. e1904113.
(43) He, X.; Yang, S.; Pei, Q.; Song, Y.; Liu, C.; Xu, T.; Zhang, X. Integrated Smart Janus Textile Bands for Self-Pumping Sweat Sampling and Analysis. *ACS Sens* **2020**, *5*, 1548−1554.
(44) Li, Y.; Wang, S.; Zhang, J.; Ma, X.; Cao, S.; Sun, Y.; Feng, S.; Fang, T.; Kong, D. A Highly Stretchable and Permeable Liquid Metal Micromesh Conductor by Physical Deposition for Epidermal Electronics. *ACS Appl. Mater. Interfaces* **2022**, *14*, 13713−13721.
(45) Feng, L.; Li, S.; Li, Y.; Li, H.; Zhang, L.; Zhai, J.; Song, Y.; Liu, B.; Jiang, L.; Zhu, D. Super-Hydrophobic Surfaces: From Natural to Artificial. *Adv. Mater.* **2002**, *14*, 1857−1860.
(46) Koch, K.; Bhushan, B.; Jung, Y. C.; Barthlott, W. Fabrication of Artificial Lotus Leaves and Significance of Hierarchical Structure for Superhydrophobicity and Low Adhesion. *Soft Matter* **2009**, *5*, 1386−1393.
(47) Han, L.; Mao, Z.; Wu, J.; Guo, Y.; Ren, T.; Gao, C. Directional Cell Migration Through Cell-cell Interaction on Polyelectrolyte Multilayers with Swelling Gradients. *Biomaterials* **2013**, *34*, 975−84.
(48) Vesel, A.; Mozetic, M. Surface Modification and Ageing of PMMA Polymer by Oxygen PlasmaTreatment. *Vacuum* **2012**, *86*, 634−637.
(49) Chan, C.-M.; Hiraoka, T.-M. K. H. Polymer Surface Modification by Plasmas and Photons. *Surf. Sci. Rep.* **1996**, *24*, 1−54.
(50) Mortazavi, M.; Nosonovsky, M. A Model for Diffusion-Driven Hydrophobic Recovery in Plasma Treated Polymers. *Appl. Surf. Sci.* **2012**, *258*, 6876−6883.
(51) Jokinen, V.; Suvanto, P.; Franssila, S. Oxygen and Nitrogen Plasma Hydrophilization and Hydrophobic Recovery of Polymers. *Biomicrofluidics* **2012**, *6*, 16501−1650110.
(52) Wu, D.; Luo, Y.; Zhou, X.; Dai, Z.; Lin, B. Multilayer Poly(vinyl alcohol)-Adsorbed Coating on Poly(dimethylsiloxane) Microfluidic Chips for Biopolymer Separation. *Electrophoresis* **2005**, *26*, 211−218.
(53) Trantidou, T.; Elani, Y.; Parsons, E.; Ces, O. Hydrophilic Surface Modification of PDMS for Droplet Microfluidics Using a Simple, Quick, and Robust Method via PVA Deposition. *Microsyst. Nanoeng.* **2017**, *3*, 16091.
(54) Wang, Y.; Shi, Y.; Pan, L.; Yang, M.; Peng, L.; Zong, S.; Shi, Y.; Yu, G. Multifunctional Superhydrophobic Surfaces Templated from Innately Microstructured Hydrogel Matrix. *Nano Lett.* **2014**, *14*, 4803−4809.
(55) Lee, W. K.; Odom, T. W. Designing Hierarchical Nanostructures from Conformable and Deformable Thin Materials. *ACS Nano* **2019**, *13*, 6170−6177.
(56) Wu, J.; Wang, N.; Wang, L.; Dong, H.; Zhao, Y.; Jiang, L. Unidirectional Water-penetration Composite Fibrous Film via Electrospinning. *Soft. Matter.* **2012**, *8*, 5996−5999.
(57) Jung, D.; Lim, C.; Park, C.; Kim, Y.; Kim, M.; Lee, S.; Lee, H.; Kim, J. H.; Hyeon, T.; Kim, D. H. Adaptive Self-Organization of Nanomaterials Enables Strain-Insensitive Resistance of Stretchable Metallic Nanocomposites. *Adv. Mater.* **2022**, *34*, 2200980.
(58) Wang, L.; Wang, L.; Zhang, Y.; Pan, J.; Li, S.; Sun, X.; Zhang, B.; Peng, H. Weaving Sensing Fibers into Electrochemical Fabric for Real-Time Health Monitoring. *Adv. Funct. Mater.* **2018**, *28*, 1804456.
(59) Wang, P.; Chen, M.; Han, H.; Fan, X.; Liu, Q.; Wang, J. Transparent and Abrasion-Resistant Superhydrophobic Coating with Robust Self-cleaning Function in either Air or Oil. *J. Mater. Chem. A* **2016**, *4*, 7869−7874.
(60) Bai, C.; Ji, K.; Wang, H.; Zhang, J.; Hu, G.; Kong, D. Intrinsically Stretchable Microbattery with Ultrahigh Deformability for Self-Powering Wearable Electronics. *ACS Mater. Lett.* **2022**, *4*, 2401−2408.
(61) Bi, Y.; Ye, J. In Situ Oxidation Synthesis of Ag/AgCl Core-shell Nanowires and Their Photocatalytic Properties. *Chem. Commun.* **2009**, 6551−6553.

https://doi.org/10.1021/acsnano.3c10324
ACS Nano 2024, 18, 2335−2345